

Article

Large-Scale Physical Modeling of Salt-Water Intrusion

Elena Crestani ^{1,*}, Matteo Camporese ¹, Enrica Belluco ¹, Abderrezak Bouchedda ², Erwan Gloaguen ²
and Paolo Salandin ¹

¹ Department of Civil, Environmental and Architectural Engineering, University of Padova, 35131 Padova, Italy; matteo.camporese@unipd.it (M.C.); enrica.belluco@unipd.it (E.B.); paolo.salandin@unipd.it (P.S.)

² Centre Eau Terre Environnement, Institut National de la Recherche Scientifique,

Quebec City, QC G1K 9A9, Canada; abderrezak.bouchedda@ete.inrs.ca (A.B.); erwan.gloaguen@inrs.ca (E.G.)

* Correspondence: elena.crestani@unipd.it

Abstract: Salt-water intrusion (SWI) is a worldwide problem increasingly affecting coastal aquifers, exacerbated by climate changes and growing demand of fresh-water. Therefore, research on this topic using both physical and numerical modeling has been intensified, aiming to achieve better predictions of the salt-water wedge evolution and to design suitable countermeasures to its negative effects. This work presents a laboratory facility designed to conduct SWI experiments that can be used as benchmarks for numerical models. To this end, the laboratory facility has been designed to limit errors and provide redundant measurements of hydraulic heads and discharged flow rates. Moreover, the size of the facility allows us to monitor the salt-water wedge evolution by a specifically designed electrical resistivity tomography (ERT) monitoring system. To demonstrate the capabilities of the laboratory facility, we carried out a simple 36-h long SWI experiment in a homogeneous porous medium: during the initial 24 h the salt-water wedge evolved without any external forcing, while in the last 12 h, fresh-water was pumped out to simulate aquifer exploitation. The experiment was monitored through ERT and photos of the salt-water wedge collected at regular time intervals. The SUTRA code was used to reproduce the experimental results, by calibrating only the dispersivities. The ERT results show a good correlation with simulated concentrations between the borehole electrodes, the most sensitive zone of the monitored area, demonstrating that ERT can be used for laboratory evaluations of the salt-water evolution. Overall, the agreement between observed data, numerical simulations, and ERT results demonstrates that the proposed laboratory facility can provide valuable benchmarks for future studies of SWI, even in more complex settings.

Keywords: salt-water intrusion; laboratory experiment; electrical resistivity tomography; aquifer exploitation



Citation: Crestani, E.; Camporese, M.; Belluco, E.; Bouchedda, A.; Gloaguen, E.; Salandin, P. Large-Scale Physical Modeling of Salt-Water Intrusion. *Water* **2022**, *14*, 1183. <https://doi.org/10.3390/w14081183>

Academic Editors: Jiabi Du and Jian Shen

Received: 8 March 2022

Accepted: 4 April 2022

Published: 7 April 2022

Publisher's Note: MDPI stays neutral with regard to jurisdictional claims in published maps and institutional affiliations.



Copyright: © 2022 by the authors. Licensee MDPI, Basel, Switzerland. This article is an open access article distributed under the terms and conditions of the Creative Commons Attribution (CC BY) license (<https://creativecommons.org/licenses/by/4.0/>).

1. Introduction

Seawater intrusion in coastal aquifers is a worldwide problem caused, among other factors, by aquifer overexploitation related to human activities, such as irrigation and drinking water supply, and the reduction in natural groundwater recharge due to climate change [1]. To prevent or limit the deterioration of both surface water and groundwater quality due to salt-water contamination, research studies have been developed to fully comprehend the problem and identify its fundamental parameters, as well as to evaluate possible countermeasures, such as cut-off walls (e.g., [2–12]).

Within this context, physical models represent a fundamental tool for studying seawater intrusion and evaluating the effectiveness of solutions to limit the salt wedge, while keeping under control system parameters, such as soil and water characteristics, as well as initial and boundary conditions. For instance, Zhang et al. [13] carried out, for the first time, an experiment to simulate a contaminant intrusion from a surface source in a coastal aquifer. Goswami and Clement [14] carried out laboratory experiments to generate quantitative datasets to describe the transport patterns of intruding and receding salt

wedges under different hydraulic gradients and with particular attention to the transient conditions. The results were then compared with numerical solutions obtained with the SEAWAT code [15]. Werner et al. [16] developed a controlled laboratory experiment to reproduce the upcoming phenomenon in two dimensions, with different pumping rates and different fresh-water–salt-water densities, to compare the experimental results with the analytical solutions by Dagan and Bear [17]. The results by Werner et al. [16] were then analyzed by Jakovovic et al. [18] with a density-dependent flow and transport model to explore the temporal development of experimental salt-water plumes. Many other studies used combinations of laboratory experiments and numerical models to study issues linked to seawater intrusion: Chang and Clement in [19,20] focused on the impacts of recharge fluxes variations and dynamics of groundwater flow and transport processes within the salt-water wedge, respectively; Morgan et al. [21] reproduced the phenomenon of seawater intrusion overshoot; Mehdizadeh et al. [22] simulated various pumping scenarios in order to verify the validity of a sharp-interface assumption; Luyun et al. in [2,3] analyzed the performance of subsurface cut off walls and recharge wells as possible countermeasures to seawater intrusion; more recently Na et al. [23] studied the influence of seawater density variations on seawater intrusion.

In the previously mentioned studies, the experiments were monitored by taking regular camera images of the salt-water wedge, highlighted by adding dye to the salt-water. The same technique was used by Robinson et al. [24], who developed a method for automatic image analysis to convert the image light intensity to concentrations, and by Abdoulhalik et al. [5] and Abdoulhalik and Ahmed [25], in a small scale laboratory experiment to study the effects of underground barriers in homogeneous aquifers and of a cut-off wall in a heterogeneous aquifer. On the other hand, Abdollahi-Nasab et al. [26] were able to investigate the flushing of salt-water by fresh-water, propagating seaward, monitoring the experiment by using only pressure transducers and conductivity meters.

A common feature of the aforementioned experiments is that they were carried out in flumes or sandboxes of limited size, both in terms of length and width, the former being typically less than 1 m, with a few exceptions (e.g., [27–29]), and the latter being usually less than 10 cm, and even as small as 1 or 2 cm. On one hand, small widths imply that the wall effect, whereby the lateral walls represent preferential flow paths due to the relatively higher hydraulic conductivity and lower dispersivity compared to the porous media (e.g., [30]), plays a major role. On the other hand, measurements in short flumes can be significantly affected by an imperfect definition of the initial conditions or possible head fluctuations at the inland and seaward boundaries, making a correct definition of the gradient uncertain (e.g., [31]).

The objective of this paper is to introduce a large laboratory facility designed and built to reproduce salt-water intrusion in coastal aquifers. The use of a large flume allows us to limit measurements relative errors, to minimize the wall effects and to use the electrical resistivity tomography (ERT) (e.g., [32–39]), as an alternative technique to monitor the evolution of the salt-water wedge, thanks to the large resistivity contrast between salt-water and fresh-water.

The capabilities of our laboratory facility are here demonstrated for a 36 h experiment of seawater intrusion within a homogeneous porous medium, including water pumping from a channel drain in the last 12 h. The salt wedge evolution was monitored by collecting photographs at regular intervals and by an ERT survey with a joint surface and cross-borehole configuration, specifically designed for the laboratory flume. The experimental results given by photographic evidence and the ERT survey were then compared with simulations by the SUTRA code [40].

2. Material and Methods

2.1. Experimental Methods

2.1.1. The Sandbox Setup

The sandbox used in this study is schematized in Figure 1 and measures 500 cm long by 30 cm wide by 60 cm high, with 3 cm thick plexiglass walls. Two tanks are located upstream and downstream from the sandbox, with volumes of 0.32 m³ and 1.6 m³, respectively. The upstream tank is filled with fresh-water and is continuously supplied by a small pump, providing fresh-water recharge. The downstream tank is filled with salt-water, previously prepared by adding salt to fresh-water till a proper density is reached, and it represents the sea. Both tanks are equipped with a spillway that, by discharging the excess flow, guarantees a constant water level, which is also continuously measured by ultrasonic sensors, allowing us to monitor the gradient and to check that it does not change or fluctuate during the experiment. Red food dye is added to the salt-water to easily visualize the salt wedge. Preliminary analyses, not shown here, were carried out on the dye to verify its ability to be used as a tracer for the salt-water and a good correlation between measured light absorbance and salt concentration in terms of electrical conductivity was found [41].

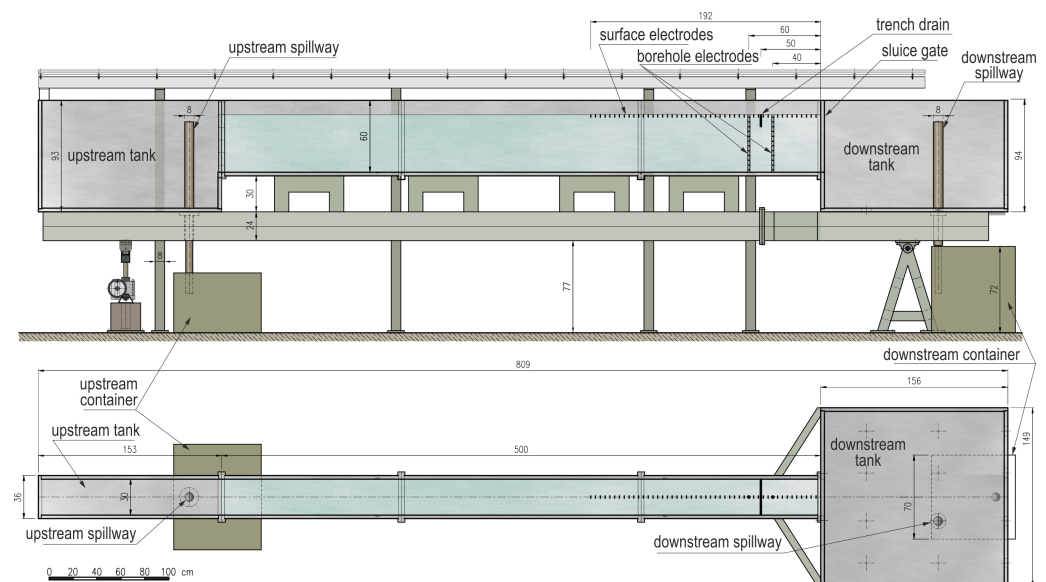


Figure 1. Schematic lateral (**top**) and plan (**bottom**) views of the sandbox (all distances are expressed in cm).

The porous medium in the sandbox is obtained by means of glass beads, as commonly adopted in previous studies (e.g., [2,14,20,24]). The main advantage of using glass beads is the absence of chemical interactions between the dye and salt mixture with the porous matrix, which allows for multiple test repetitions. The beads are characterized by a nominal size range equal to 0.4–0.8 mm, a median diameter d_{50} of 0.6 mm, and a uniformity coefficient of $d_{60}/d_{10} \approx 1.5$, corresponding to a fairly homogeneous material. The porous medium was packed into the sandbox under moist conditions (e.g., [42]): the beads were arranged layer by layer by compacting each 5-cm stratum with a 4-kg weight falling from a height of 20 cm.

A channel drain was added to the system, in order to simulate a fresh-water withdrawal close to the coastal line, as in real world cases. The channel drain is located 50 cm upstream from the salt-water tank and it is 30 cm long (intercepting the whole sandbox width), 1 cm wide and 10 cm deep. This depth ensures that the water table is always intercepted with or without water extraction. The channel drain is made of plexiglass and fiberglass, including a plastic mesh that prevents the glass beads to enter into the device.

Prior to the experiment, the porous medium was saturated with fresh-water by very slowly increasing the water level in both tanks, to avoid the formation of air bubbles, and then keeping the water level higher than the porous medium height, i.e., 48 cm, for at least two weeks. When the saturation was completed, some constant-head tests were performed with different hydraulic gradients, in order to estimate the saturated hydraulic conductivity K . All the tests converged to a K value of approximately 1.3×10^{-3} m/s.

2.1.2. Monitoring Equipment

Acoustic probes (Pepperl + Fuchs UC500-30GM-IUR2-V15), with data collection frequency of 30 Hz, were used to monitor the water level in the upstream and downstream tanks, and to measure the discharge flow rate. To this aim, the water discharged from the spillway in the downstream tank was collected in a calibrated container, with area A_{cont} , placed under the tank, and the flow rate $Q_{disch\ exp}$ was derived from measurements of the water level variation Δh recorded every 10 min. The system setup was designed to guarantee relatively constant flow conditions throughout the experiment.

The fresh-water inflow was always small compared to the capacity of the downstream tank (about 5% of its volume), in order to avoid a significant dilution of the salt-water. Nonetheless, to verify this, water electrical conductivity was measured in the downstream tank every 20 min by a portable conductivity meter (WTW Multiline P4).

The salt-water wedge evolution was monitored with two different methods: (i) Photographs of the red-colored wedge were collected at a 5-min interval with a Nikon D7000 camera, for a total of 432 photographs; (ii) Electrical resistivity tomography (ERT) was used to derive images of electrical resistivity distributions every 20 min, for a total of 108 measures.

2.1.3. ERT Monitoring and Inversion Modeling

The ERT time-lapse surveys were carried out using 73 electrodes placed in two boreholes and one surface profile along the center axis of the sandbox (Figure 1). The ERT data were measured with a joint surface, surface-to-borehole and cross-borehole configurations, specifically designed for the laboratory flume. Boreholes were built using two slotted PVC tubes of 17 mm diameter. Surface electrodes are cylindrical gold-plated metal electrodes of 0.015 m length, whereas borehole ring electrodes are made of stainless steel metal to minimize the corrosion due to the highly conductive solution. The surface profile is 1.9 m long, consisting of 48 electrodes inserted into the porous medium at regular spacing of 0.04 m. The first and the last electrodes of the profile are located at 1.96 m and 0.08 m from the downstream end of the flume, respectively. In order to use a pole-dipole array, the infinite electrode was placed in the opposite side of the downstream end of the flume at 0.06 m from the fresh-water tank, i.e., 2.98 m from the first profile electrode. To increase the sensitivity and improve the resolution of ERT to the salt-water wedge at depth, two boreholes were placed at 0.40 m and 0.60 m from the downstream salt-water tank. In each borehole, 12 electrodes were placed from 0 to 0.48 m depth at 0.04 m interval. Note that the equivalent hydraulic conductivity of the slotted wells is larger than the one of the porous medium, as verified by preliminary infiltration tests (not shown here). On the other hand, the size of the slots is small enough to prevent the glass beads entering into the boreholes. Raw ERT data were collected every 20 min using an IRIS Syscal Pro 72 Switch resistivity meter (France). Each time-lapse data acquisition takes approximately 7 min, a very short time compared to the dynamics of the salt wedge, which allows us to capture instant snapshots of electrical images. The ERT data measurement protocol consists of 3315 different combinations of surface pole-dipole array, cross-borehole, and surface-to-borehole measurements in both pole-dipole and dipole-dipole configurations [43].

Although the groundwater flow modeling is conducted in 2D (Section 2.2), the ERT forward problem is 3D because the sand box width (0.3 m) is small compared to the ERT profile length (1.9 m). Therefore, large electrode spacing data measurements are not only affected by medium resistivity changes but also by the sandbox walls, whose effect on data

measurements is not constant with time because of nonlinearity and non-uniqueness of the ERT inverse problem. This is generally solved using nonlinear regularization using smoothness constraints [44]. In this work, we used E4D [45], a three-dimensional resistivity inversion and finite elements modeling software using tetrahedral mesh elements. The conductivity model of the sandbox experiment was discretized, as shown in Figure 2. Fresh-water and salt-water tanks are located from $x = -1$ m to 0 m and from $x = 6$ m to 5 m, respectively. Their electrical conductivity values were kept fixed to 0.06 S/m and 6.73 S/m, respectively, during the inversion. Boundary conditions of null conductivity are assigned at the sandbox walls and bottom. The infinite electrode for the pole-dipole array is located at $x = 0.06$ m and the surface profile starts at $x = 3.04$ m and ends at $x = 4.92$ m.

As shown in Figure 2, the initial electrical conductivity distribution is uniform for all the inversions. Goebel et al. [46] demonstrated that incorporating prior information, such as the shape of the salt-water wedge, in the initial guess can significantly improve the inverted solution. However, we elected to use the worst case scenario in which no prior information about the salt-water wedge is available, to better represent conditions more likely encountered in field surveys. As an additional result of the inversions, E4D also provides the cumulative sensitivity of the conductivity values, corresponding to the diagonal of the iterative inversion scheme Jacobian matrix (e.g., [47]).

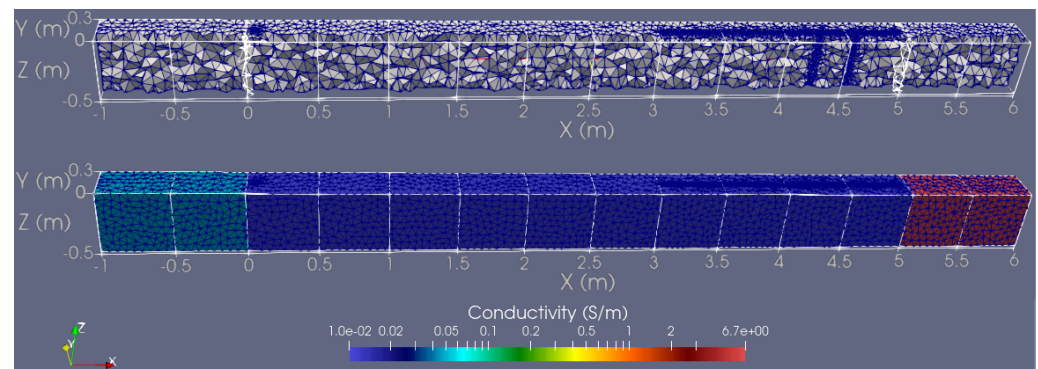


Figure 2. (top) Vertical cross-section at $y = 0.15$ m of the finite element mesh used for the electrical resistivity tomography (ERT) inversions. (bottom) Initial distribution of electrical conductivities. The conductivities of the fresh-water tank and salt-water tank were kept fixed at values of 0.06 and 6.73 S/m, respectively. Some like $1.0e-02$ mean 1.0×10^{-2} .

2.1.4. Experiment Set-Up and Initialization

The experiment was characterized by a hydraulic gradient of about 0.39%, a small value that can be representative of real field conditions (e.g., [48,49]). This gradient could be obtained here thanks to the large size of the flume and, thus, the relatively limited errors in the hydraulic head measurements. As a result, the corresponding discharge flow rate was also small, of the order of 1.6 L/h when the channel drain was not activated and 0.3 L/h when it was pumping out fresh-water.

The water density, measured both by densimeter and weight of a known volume, was equal to 1000 and 1026 kg/m^3 for fresh-water and salt-water, respectively.

The electrical conductivity measured during the whole experiment in the downstream tank remained constant (average value of 6.8 S/m and standard deviation of 0.18 mS/cm), demonstrating that no significant salt dilution occurred, being the integral volume of fresh-water released during the experiment negligible compared to the salt-water tank capacity.

Due to the large size of the seaward tank, it was not possible to fill it instantaneously by a tracer slug, as performed in previous studies (e.g., [14]). Therefore, our initialization procedure was more complex. Initially, a flow of fresh-water was only driven by a gradient of $0.39\% \pm 0.01\%$, keeping a seaward saturated thickness of 42 cm. This was maintained for 24 h to ensure the achievement of steady state hydraulic flow conditions and to double-check the hydraulic conductivity and discharged flow rate values before the

experiment. Then, the closure of a sluice gate (Figure 1), installed between the sandbox and the downstream tank, allowed the replacement of fresh-water with salt-water in the downstream tank, up to the original level. These operations lasted about 20 min, during which the fresh-water flow stopped, and the water in the sandbox leveled off. Then, the sluice gate was quickly lifted and the salt-water wedge was allowed to infiltrate into the porous medium, effectively marking the start of the salt-water intrusion experiment.

2.2. Numerical Modeling

The salt-water intrusion experiment was reproduced by using SUTRA (Saturated–unsaturated transport) [40], a well-established numerical model that can simulate saturated–unsaturated and density-dependent groundwater flow based on quadrilateral finite elements.

The computational domain, representing the sandbox, was discretized by a total of 237,500 elements, corresponding to 1250 by 190 quadrilaterals along the horizontal and vertical directions, respectively. Two different element sizes were used ($0.25\text{ cm} \times 1\text{ cm}$ and $0.25\text{ cm} \times 0.25\text{ cm}$), with the smaller elements closer to the downstream tank, wherein the salt-water wedge mostly evolves.

The porous medium was assumed homogeneous, with K equal to $1.3 \times 10^{-3}\text{ m/s}$ and porosity $n = 0.37$. The water density was also assigned on the basis of measured values, equal to 1000 and 1026 kg/m^3 for fresh-water and salt-water, respectively.

The unsaturated zone in the experiment is not relevant, as its mean thickness is 6 cm, compared to a total thickness of the porous medium of 48 cm, and because no infiltration from the top occurred during the experiment. It is then described in the model by a generic fine sand retention curve.

The channel drain is simulated by means of elements characterized by a hydraulic conductivity value three orders of magnitude larger than the porous medium.

The simulation time step was 1 min. The initial conditions for the simulation correspond to the experimental system state resulting from the sluice gate operations carried out to fill the downstream tank with salt-water and that temporarily stopped the fresh-water flow.

The boundary conditions were assigned in accordance with Abarca et al. [50] by imposing a global flux condition on both fresh-water and salt-water fluxes that reflects the conditions observed during the experiment.

The longitudinal (α_L) and transversal (α_T) dispersivity coefficients were the only parameters calibrated by fitting the modeled salt wedge shape and toe position to the observed data. The resulting values ($\alpha_L = 0.001\text{ m}$ and $\alpha_T = 0.0001\text{ m}$) are consistent with the guidelines based on the mesh-based Péclet number, as indicated by Voss and Provost [51], and with values found in the literature (e.g., [14,22,52–54]).

3. Results

We describe here the experimental and modeling results of the two phases of the experiment, the first one without external forcing and the second one with water pumping from the channel drain.

The main experiment parameters are summarized in Table 1, while Figure 3 reports the mean values of the discharged ($Q_{disch\ exp}$) and pumped ($Q_{trench\ exp}$) flow rates measured throughout the experiment as compared to the corresponding modeled flow rates. Figure 3 also shows the modeled exiting fresh-water flow rate Q_{fresh} and entering salt-water flow rate Q_{salt} , whose difference gives the Q_{disch} , and the modeled Q_{in} , i.e., the sum of Q_{disch} and Q_{trench} . The two phases are clearly distinguishable in the Figure, the second one (with pumping) being characterized by an increase in salt-water flux entering the porous medium, a decrease in fresh-water discharge and an overall slight increase in the inflow, due to a larger local gradient caused by pumping.

Table 1. Summary of the variables and parameters of the physical and numerical models.

Variable or Parameter	Symbol	Value	Type
Porous Medium thickness	B	0.48 m	measured
Hydraulic gradient		0.0039	measured
Seaward water depth		42 cm	measured
Hydraulic conductivity	K	1.30×10^{-3} m/s	measured
Discharged flow rate (first phase)	$Q_{disch\ exp}$	1.6 L/h	measured
Discharged flow rate (second phase)	$Q_{disch\ exp}$	0.3 L/h	measured
Pumped flow rate	$Q_{trench\ exp}$	1.3 L/h	measured
Porosity	n	0.37	measured
Longitudinal dispersivity	α_L	0.001 m	calibrated
Transversal dispersivity	α_T	0.0001 m	calibrated

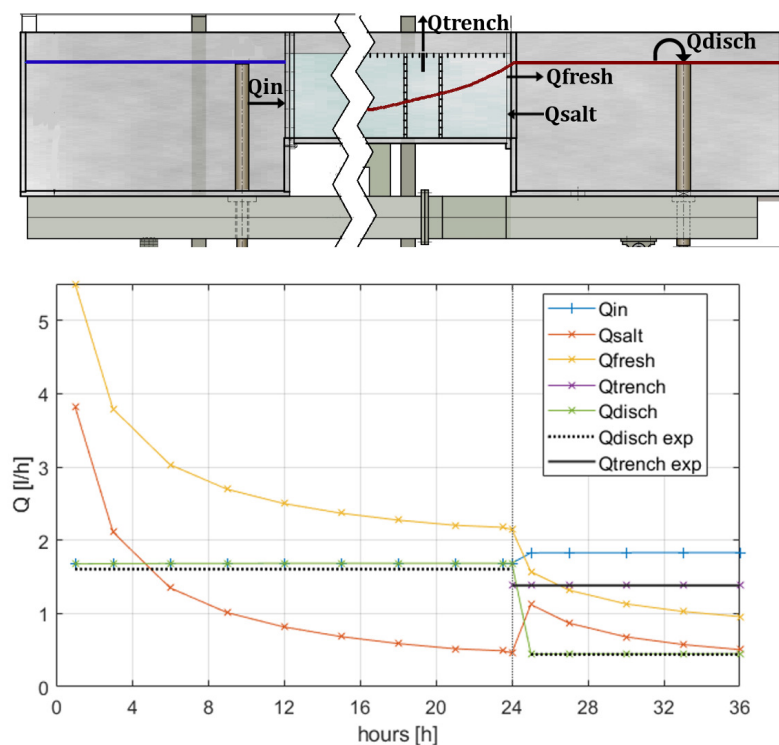


Figure 3. (top) Schematization of the flow partitioning in the sandbox and (bottom) the simulated flow rates and the mean measured experimental flow rates as represented in the scheme. The grey vertical dotted line indicates when pumping starts.

3.1. First Phase: No Pumping

The salt-water wedge at 24 h since the opening of the sluice gate can be visualized in Figure 4 as photographed by the camera and in terms of electrical resistivity distribution derived by the ERT inversion. In the latter, the grey dashed lines delimit the area where the ERT inversion is more reliable. Outside that area the ERT inversion results are much less meaningful and the result analysis should refer only to the photograph. The numerical result is superimposed on both the experimental results: the thin white region represents the wedge shape as computed by the numerical model, defined here as the bounded contours with concentration between 20% and 80% of the salt-water concentration.

To properly analyze the ERT results, we need to consider that the last electrode is located at $x = 4.92$ m. Hence, there is no information between $x = 4.92$ m and 5 m, which explains the difference between electrical conductivity and concentration images at this location. Additionally, outside the region encompassed by the boreholes the electrical conductivity distribution is affected by overdispersion, due to the poor resolution at depth.

Nonetheless, the overall shape of the salt-water wedge is captured by the ERT image, the best inversion results being obtained between the two boreholes and in the middle of the sandbox at $y = 0.15$ m, where the sensitivity to the measurements is higher. This is not surprising, as it is well known that ERT sensitivity decreases quickly by moving away from the electrodes.

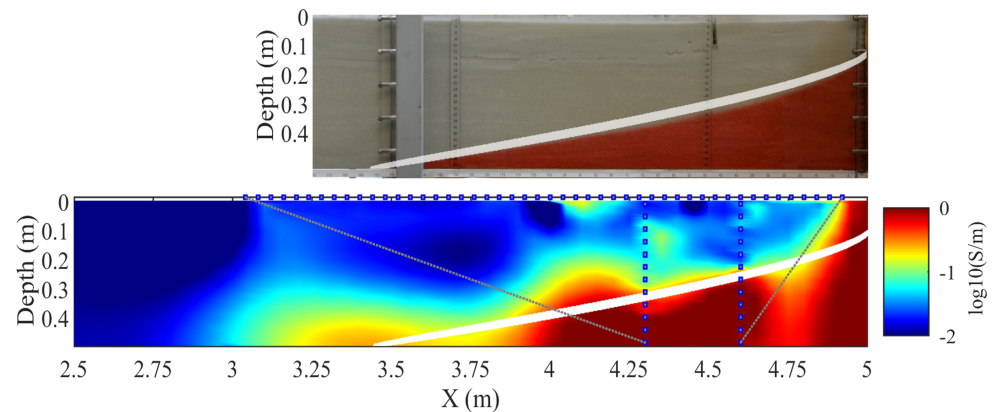


Figure 4. Illustration of the salt-water wedge after 24 h from the beginning of the experiment: (top) photograph, (bottom) electrical resistivity distribution as computed by the ERT inversion. The thin white region superimposed on both images represents the wedge transition zone as computed by the numerical model. The grey dashed lines delimit the area where ERT inversions are more reliable, due to larger sensitivities.

A quantitative assessment of the correlation between simulated concentrations and electrical conductivity values from ERT inversions is given by the scatter plot in Figure 5. As the grid used for computing the concentrations is finer (0.0025×0.0025 m²) than the one used for the electrical conductivities ($0.025 \times 0.025 \times 0.025$ m³), the concentration values are averaged over the cells of the electrical model grid. To show the effect of ERT sensitivity on the relationship between estimated electrical conductivity and simulated salt concentration, the cumulative sensitivity for each conductivity cell is calculated and normalized by the maximum value. Figure 5 shows that the correlation coefficient between electrical conductivities and salt concentrations increases from 0.32 to 0.68 if only the conductivity data with normalized sensitivity larger than 0.4 is taken into account.

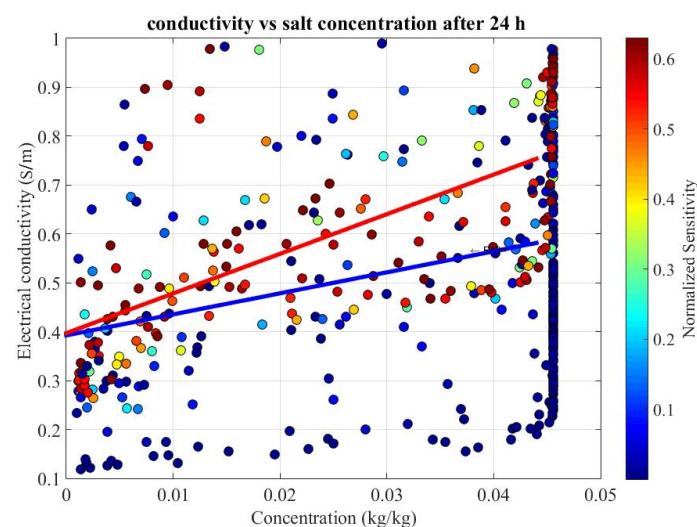


Figure 5. Scatter plot between electrical conductivity values and concentration values at 24 h. The blue and red lines represent the linear regression carried out using all the data and the data with normalized sensitivity >0.4 , respectively.

Overall, the qualitative correspondence between salt wedge as captured by the photograph, the SUTRA simulation, and the ERT inversions is quite good, despite the limitations of ERT outside the most sensitive zone between the boreholes. The main differences concern the transition zone between fresh-water and salt-water: while the ERT image shows the presence of a mixing zone, the photo exhibits a very sharp interface, without visible evidence of a mixing zone. This may be due to the fact that the camera is only able to capture what is happening at the contact between the fluid and the plexiglass, preventing the visual identification of a mixing zone. On the other hand, the presence of a diffusive zone in the ERT image may be due to overdispersion that typically affects ERT inversion products (e.g., [47,55]).

3.2. Second Phase: Pumping from the Channel Drain

After 24 h from the beginning of the experiment, water pumping through the channel drain was activated, causing a reduction in the fresh-water flow downstream of the channel drain. This is a realistic reproduction of a common situation in coastal aquifers exploited for drinking water supply and irrigation.

Figure 6 shows a photograph of the sandbox after 8 h of pumping (i.e., after 32 h from the beginning of the experiment) and the corresponding electrical resistivity distribution inverted from the ERT data, both overlapped with the numerical result.

A slight upcoming effect due to the pumping is visible in the ERT image, between the boreholes, and in the model simulation, while just a hint can be deduced from the photograph. This could be due again to the lack of a visible transition zone in the photograph, as discussed in the previous section, and highlights the need to combine different measurements techniques as proposed here.

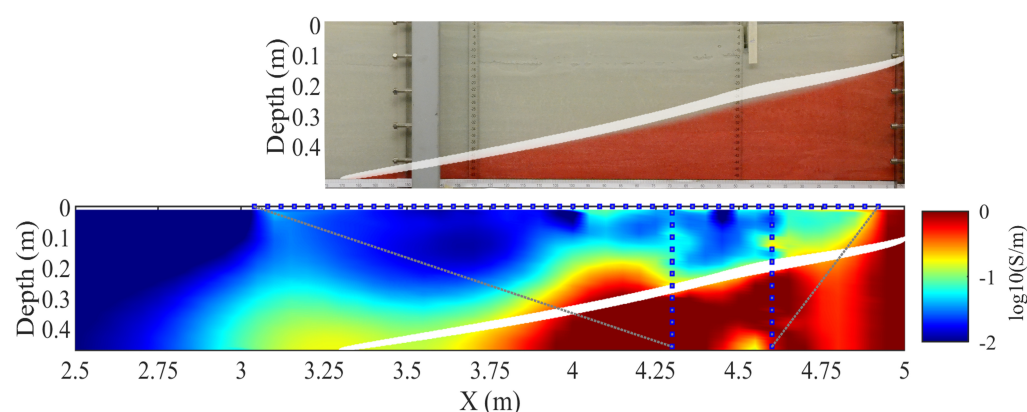


Figure 6. Illustration of the salt-water wedge after 32 h from the beginning of the experiment: (top) photograph, (bottom) electrical resistivity distribution as computed by the ERT inversion. The thin white region superimposed on both images represents the wedge transition zone as computed by the numerical model. The grey dashed lines delimit the area where ERT inversions are more reliable, due to larger sensitivities.

In Figure 7, the scatter plot between simulated salt concentration and estimated electrical conductivity, analogous to Figure 5, is shown. The linear regression is carried out using all data (blue line) and only data with normalized sensitivity larger than 0.4 (red line): the resulting correlation coefficients are 0.69 and 0.88, respectively, confirming the good performance of the ERT in the region between the boreholes. The higher correlation coefficients than in the case without pumping depend from the fact that at 32 h the salt-water wedge covers a larger portion of the sandbox than at 24 h, and, therefore, the area investigated by the ERT is characterized by higher electrical conductivities, that determine smaller electrical inversion errors and then higher correlation between electrical conductivity and concentration than at 24 h.

Both numerical results and ERT evidence show how water pumping caused a local increase in the transition zone thickness, especially at a distance of 40 cm from the seaward boundary. This effect gradually reduces as the distance from the downstream tank increases. These findings are consistent with numerical results reported in the literature [56].

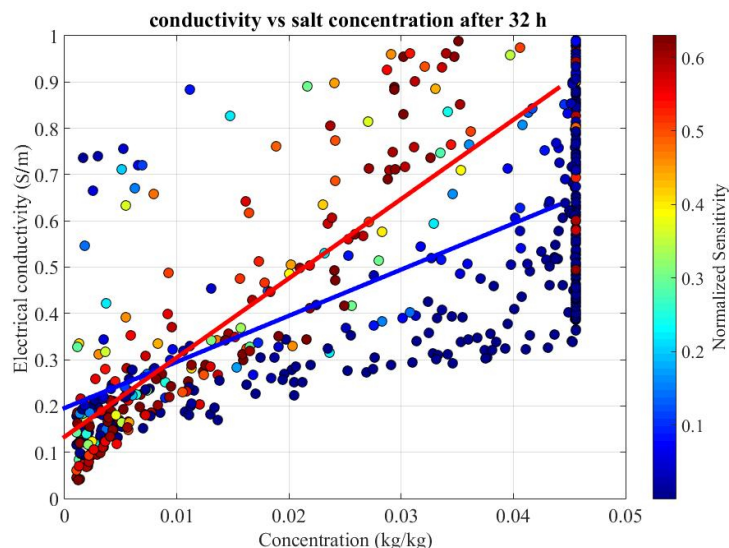


Figure 7. Scatter plot between electrical conductivity values and concentration values at 32 h (8 h of pumping). The blue and red lines represent the linear regression carried out using all the data and the data with normalized sensitivity >0.4 , respectively.

4. Summary and Conclusions

In this paper, we presented a laboratory facility designed to carry out experiments of seawater intrusion in coastal aquifers to serve as potential benchmarks for numerical models. As a demonstration of its capabilities, we carried out an experiment in a homogeneous porous medium considering the salt wedge evolution driven by the instantaneous application of a constant seaward boundary condition in a free surface aquifer characterized by a constant gradient. Fresh-water pumping from a surface channel drain crossing the entire width of the aquifer was also considered. The experimental findings were then reproduced with the SUTRA code, whereby only the longitudinal and transversal dispersivities were adjusted to fit the shape and advancement of the salt wedge toe, while all the other model parameters were assigned based on the experimental data.

The width and length of our laboratory facility, i.e., a specifically designed sandbox, are, to the best of our knowledge, larger than most of the others used for the same purpose, allowing for the use of electrical resistivity tomography (ERT), with a joint surface and cross-borehole configuration, as a quantitative monitoring tool. The flume length of 500 cm allows the salt wedge to span hundred of centimeters during long experiments, making the effects of possible head fluctuations at the inland and seaward boundaries and uncertainties on the initial conditions negligible. Furthermore, our experimental conditions are highly controlled and the main factors affecting the salt-water intrusion can be monitored for the entire experiment duration. The hydraulic gradient, the discharged flow rate and the water electrical conductivity in the downstream tank are continuously measured, while the hydraulic conductivity can be determined through constant-head tests, resulting in an experimental system with redundant measurements and a careful definition of their uncertainty.

The approach we suggest to monitor the salt-water wedge evolution is a combination of two complementary methods. The visual observation of the salt-water intrusion, by means of photographs taken at regular time intervals, allows us to check the toe wedge position but may be affected by errors related to wall effect phenomena and light refraction, that makes it difficult to identify the transition zone. In order to overcome these issues

and to achieve a more comprehensive description of the process, a properly designed ERT system can be used to monitor the evolution of the salt-water wedge. The ERT inversions showed here are promising: despite a significant dispersion typical of the ERT inversions and despite the fact that we performed the inversion assuming no prior information about the salt-water shape evolution, we found statistically significant correlations between the salt concentrations simulated by SUTRA and inverted electrical conductivity values, which also showed evidence of the presence of a transition zone. Overall, the ERT results proved to be effective in highlighting the effects of the pumping, especially between the boreholes suggesting that a surface-electrode only configuration, due to low sensitivity at depth, is not suitable to accurately monitor the evolution of the salt-water wedge.

The numerical simulations were set up to reproduce exactly the laboratory experiment in all its phases, including the preliminary aquifer saturation and downstream tank fill-up. The simulation results were in very good agreement with the experimental observations confirming that our experimental facility can be used to develop benchmarks for the validation of density-dependent flow and transport numerical models.

Future directions of the research will include an increase in the number of boreholes, to improve the effectiveness of the ERT monitoring system, and the investigation of the effects and performance of cut-off walls as possible countermeasures to seawater intrusion, also in a more realistic set-up with heterogeneous porous media.

Author Contributions: Conceptualization, E.C., M.C. and P.S.; data curation, E.C., E.B. and A.B.; formal analysis, E.C., M.C., E.G. and P.S.; funding acquisition, P.S.; investigation, E.C., E.B. and A.B.; methodology, M.C., E.G. and P.S.; software, E.C., E.B. and A.B.; supervision, M.C., E.G. and P.S.; writing—original draft preparation, E.C.; writing—review and editing, M.C., E.G. and P.S. All authors have read and agreed to the published version of the manuscript.

Funding: This research was funded by the contribution from the EU co-financing and the Interreg Italy–Croatia Cross Border Collaboration (CBC) Programme 2014–2020 (Priority Axes: Safety and Resilience) through the European Regional Development Fund as a part of the project “Monitoring seawater intrusion in coastal aquifers and testing pilot projects for its mitigation” (MoST) (AID: 10047743).

Institutional Review Board Statement: Not applicable.

Informed Consent Statement: Not applicable.

Data Availability Statement: Under request to the corresponding author.

Acknowledgments: Figure 2 was made with the open-source software ParaView.

Conflicts of Interest: The authors declare no conflict of interest.

References

1. Ketabchi, H.; Mahmoodzadeh, D.; Ataie-Ashtiani, B.; Simmons, C.T. Sea-level rise impacts on seawater intrusion in coastal aquifers: Review and integration. *J. Hydrol.* **2016**, *535*, 235–255. [[CrossRef](#)]
2. Luyun, R.; Momii, K.; Nakagawa, K. Laboratory-scale saltwater behavior due to subsurface cutoff wall. *J. Hydrol.* **2009**, *377*, 227–236. [[CrossRef](#)]
3. Luyun, R.; Momii, K.; Nakagawa, K. Effects of Recharge Wells and Flow Barriers on Seawater Intrusion. *Ground Water* **2011**, *49*, 239–249. [[CrossRef](#)]
4. Kaleris, V.K.; Ziogas, A.I. The effect of cutoff walls on saltwater intrusion and groundwater extraction in coastal aquifers. *J. Hydrol.* **2013**, *476*, 370–383. [[CrossRef](#)]
5. Abdoulhalik, A.; Ahmed, A.; Hamill, G. A new physical barrier system for seawater intrusion control. *J. Hydrol.* **2017**, *549*, 416–427. [[CrossRef](#)]
6. Armanuos, A.M.; Ibrahim, M.G.; Mahmud, W.E.; Takemura, J.; Yoshimura, C. Analysing the Combined Effect of Barrier Wall and Freshwater Injection Countermeasures on Controlling Saltwater Intrusion in Unconfined Coastal Aquifer Systems. *Water Resour. Manag.* **2019**, *33*, 1265–1280. [[CrossRef](#)]
7. Lu, C.; Cao, H.; Ma, J.; Shi, W.; Rathore, S.S.; Wu, J.; Luo, J. A proof-of-concept study of using a less permeable slice along the shoreline to increase fresh groundwater storage of oceanic islands: Analytical and experimental validation. *Water Resour. Res.* **2019**, *55*, 6450–6463. [[CrossRef](#)]
8. Chang, Q.; Zheng, T.; Zheng, X.; Zhang, B.; Sun, Q.; Walther, M. Effect of subsurface dams on saltwater intrusion and fresh groundwater discharge. *J. Hydrol.* **2019**, *576*, 508–519. [[CrossRef](#)]

9. Armanuos, A.M.; Al-Ansari, N.; Yaseen, Z.M. Assessing the effectiveness of using recharge wells for controlling the saltwater intrusion in unconfined coastal aquifers with sloping beds: Numerical study. *Sustainability* **2020**, *12*, 2685. [[CrossRef](#)]
10. Armanuos, A.M.; Al-Ansari, N.; Yaseen, Z.M. Underground barrier wall evaluation for controlling saltwater intrusion in sloping unconfined coastal aquifers. *Water* **2020**, *12*, 2403. [[CrossRef](#)]
11. Vats, O.P.; Sharma, B.; Stamm, J.; Bhattacharjya, R.K. Groundwater circulation well for controlling saltwater intrusion in coastal aquifers: Numerical study with experimental validation. *Water Resour. Manag.* **2020**, *34*, 3551–3563. [[CrossRef](#)]
12. Zang, Y.; Li, M. Numerical assessment of compressed air injection for mitigating seawater intrusion in a coastal unconfined aquifer. *J. Hydrol.* **2021**, *595*, 125964. [[CrossRef](#)]
13. Zhang, Q.; Volker, R.E.; Lockington, D.A. Experimental investigation of contaminant transport in coastal groundwater. *Adv. Environ. Res.* **2002**, *6*, 229–237. [[CrossRef](#)]
14. Goswami, R.R.; Clement, T.P. Laboratory-scale investigation of saltwater intrusion dynamics. *Water Resour. Res.* **2007**, *43*, W04418. [[CrossRef](#)]
15. Guo, W.; Langevin, C.D. User's guide to SEAWAT; a computer program for simulation of three-dimensional variable-density ground-water flow. In *US Geological Survey Techniques of Water Resources Investigations 6-A7*; US Geological Survey: Tallahassee, FL, USA, 2002. [[CrossRef](#)]
16. Werner, A.D.; Jakovovic, D.; Simmons, C.T. Experimental observations of saltwater up-coning. *J. Hydrol.* **2009**, *373*, 230–241. [[CrossRef](#)]
17. Dagan, G.; Bear, J. Solving the problem of local interface upconing in a coastal aquifer by the method of small perturbations. *J. Hydraul. Res.* **1968**, *6*, 15–44. [[CrossRef](#)]
18. Jakovovic, D.; Werner, A.D.; Simmons, C.T. Numerical modelling of saltwater up-coning: Comparison with experimental laboratory observations. *J. Hydrol.* **2011**, *402*, 261–273. [[CrossRef](#)]
19. Chang, S.W.; Clement, T.P. Experimental and numerical investigation of saltwater intrusion dynamics in flux-controlled groundwater systems. *Water Resour. Res.* **2012**, *48*, W09527. [[CrossRef](#)]
20. Chang, S.W.; Clement, T.P. Laboratory and numerical investigation of transport processes occurring above and within a saltwater wedge. *J. Contam. Hydrol.* **2013**, *147*, 14–24. [[CrossRef](#)]
21. Morgan, L.K.; Stoeckl, L.; Werner, A.D.; Post, V.E. An assessment of seawater intrusion overshoot using physical and numerical modeling. *Water Resour. Res.* **2013**, *49*, 6522–6526. [[CrossRef](#)]
22. Mehdizadeh, S.S.; Vafaie, F.; Abolghasemi, H. Assessment of sharp-interface approach for saltwater intrusion prediction in an unconfined coastal aquifer exposed to pumping. *Environ. Earth Sci.* **2015**, *73*, 8345–8355. [[CrossRef](#)]
23. Na, J.; Chi, B.; Zhang, Y.; Li, J.; Jiang, X. Study on the influence of seawater density variation on sea water intrusion in confined coastal aquifers. *Environ. Earth Sci.* **2019**, *78*, 669. [[CrossRef](#)]
24. Robinson, G.; Hamill, G.; Ahmed, A.A. Automated image analysis for experimental investigations of salt water intrusion in coastal aquifers. *J. Hydrol.* **2015**, *530*, 350–360. [[CrossRef](#)]
25. Abdoulhalik, A.; Ahmed, A.A. The effectiveness of cutoff walls to control saltwater intrusion in multi-layered coastal aquifers: Experimental and numerical study. *J. Environ. Manag.* **2017**, *199*, 62–73. [[CrossRef](#)]
26. Abdollahi-Nasab, A.; Boufadel, M.C.; Li, H.; Weaver, J.W. Saltwater flushing by freshwater in a laboratory beach. *J. Hydrol.* **2010**, *386*, 1–12. [[CrossRef](#)]
27. Kuan, W.K.; Jin, G.; Xin, P.; Robinson, C.; Gibbes, B.; Li, L. Tidal influence on seawater intrusion in unconfined coastal aquifers. *Water Resour. Res.* **2012**, *48*, W02502. [[CrossRef](#)]
28. Dose, E.J.; Stoeckl, L.; Houben, G.J.; Vacher, H.; Vassolo, S.; Dietrich, J.; Himmelsbach, T. Experiments and modeling of freshwater lenses in layered aquifers: Steady state interface geometry. *J. Hydrol.* **2014**, *509*, 621–630. [[CrossRef](#)]
29. Yu, X.; Xin, P.; Lu, C. Seawater intrusion and retreat in tidally-affected unconfined aquifers: Laboratory experiments and numerical simulations. *Adv. Water Resour.* **2019**, *132*, 103393. [[CrossRef](#)]
30. Somerton, C.W.; Wood, P. Effect of walls in modeling flow through porous media. *J. Hydraul. Eng.* **1988**, *114*, 1431–1448. [[CrossRef](#)]
31. Yalin, M. Fundamentals of hydraulic physical modelling. In *Recent Advances in Hydraulic Physical Modelling*; Martins, R., Ed.; Springer: Dordrecht, The Netherlands, 1989; Volume 165, pp. 1–37. [[CrossRef](#)]
32. Binley, A.; Henry-Poulter, S.; Shaw, B. Examination of Solute Transport in an Undisturbed Soil Column Using Electrical Resistance Tomography. *Water Resour. Res.* **1996**, *32*, 763–769. [[CrossRef](#)]
33. Kemna, A.; Vanderborght, J.; Kulesa, B.; Vereecken, H. Imaging and characterisation of subsurface solute transport using electrical resistivity tomography (ERT) and equivalent transport models. *J. Hydrol.* **2002**, *267*, 125–146. [[CrossRef](#)]
34. Kontar, E.A.; Ozorovich, Y.R. Geo-electromagnetic survey of the fresh/salt water interface in the coastal southeastern Sicily. *Cont. Shelf Res.* **2006**, *26-7*, 843–851. [[CrossRef](#)]
35. De Franco, R.; Biella, G.; Tosi, L.; Teatini, P.; Lozej, A.; Chiozzotto, B.; Giada, M.; Rizzetto, F.; Claude, C.; Mayer, A.; et al. Monitoring the saltwater intrusion by time lapse electrical resistivity tomography: The Chioggia test site (Venice Lagoon, Italy). *J. Appl. Geophys.* **2009**, *69*, 117–130. [[CrossRef](#)]
36. Rao, V.G.; Rao, G.T.; Surinaidu, L.; Rajesh, R.; Mahesh, J. Geophysical and geochemical approach for seawater intrusion assessment in the Godavari Delta Basin, AP, India. *Water Air Soil Pollut.* **2011**, *217*, 503–514. [[CrossRef](#)]
37. Pollock, D.; Cirpka, O.A. Fully coupled hydrogeophysical inversion of a laboratory salt tracer experiment monitored by electrical resistivity tomography. *Water Resour. Res.* **2012**, *48*, W01505. [[CrossRef](#)]

38. Crestani, E.; Camporese, M.; Salandin, P. Assessment of hydraulic conductivity distributions through assimilation of travel time data from ERT-monitored tracer tests. *Adv. Water Resour.* **2015**, *84*, 23–36. [[CrossRef](#)]
39. Bouzaglou, V.; Crestani, E.; Salandin, P.; Gloaguen, E.; Camporese, M. Ensemble Kalman filter assimilation of ERT data for numerical modeling of seawater intrusion in a laboratory experiment. *Water* **2018**, *10*, 397. [[CrossRef](#)]
40. Voss, C.I. *A Finite-Element Simulation Model for Saturated-Unsaturated, Fluid-Density-Dependent Ground-Water Flow with Energy Transport or Chemically-Reactive Single-Species Solute Transport*; US Geological Survey: Reston, VA, USA, 1984; Volume 84.
41. Bertorelle, E. Laboratory Experiments on the Saltwater Intrusion Process. Master's Thesis, University of Padova, Padova, Italy, 2014.
42. Felt, E.J. Laboratory methods of compacting granular soils. In *Symposium on Application of Soil Testing in Highway Design and Construction*; ASTM International: West Conshohocken, PA, USA, 1959; pp. 89–110.
43. Loke, M.; Wilkinson, P.; Chambers, J.; Meldrum, P. Rapid inversion of data from 2D resistivity surveys with electrode displacements. *Geophys. Prospect.* **2018**, *66*, 579–594. [[CrossRef](#)]
44. Tikhonov, A.; Arsenin, V.Y. Solutions of Ill Posed Problems. In *Bulletin (New Series) of the American Mathematical Society*; American Mathematical Society: Providence, RI, USA, 1977; Volume 1, pp. 521–524.
45. Johnson, T.C.; Versteeg, R.J.; Ward, A.; Day-Lewis, F.D.; Revil, A. Improved hydrogeophysical characterization and monitoring through parallel modeling and inversion of time-domain resistivity and induced-polarization data. *Geophysics* **2010**, *75*, WA27–WA41. [[CrossRef](#)]
46. Goebel, M.; Knight, R.; Kang, S. Enhancing the resolving ability of electrical resistivity tomography for imaging saltwater intrusion through improvements in inversion methods: A laboratory and numerical study. *Geophysics* **2021**, *86*, WB101–WB115. [[CrossRef](#)]
47. Binley, A.; Kemna, A. DC resistivity and induced polarization methods. In *Hydrogeophysics. Water Science and Technology Library*; Springer: Dordrecht, The Netherlands, 2005; Volume 50, pp. 129–156. [[CrossRef](#)]
48. Antonellini, M.; Mollema, P.; Giambastiani, B.; Bishop, K.; Caruso, L.; Minchio, A.; Pellegrini, L.; Sabia, M.; Ulazzi, E.; Gabbianelli, G. Salt water intrusion in the coastal aquifer of the southern Po Plain, Italy. *Hydrogeol. J.* **2008**, *16*, 1541–1556. [[CrossRef](#)]
49. Yechieli, Y.; Shalev, E.; Wollman, S.; Kiro, Y.; Kafri, U. Response of the Mediterranean and Dead Sea coastal aquifers to sea level variations. *Water Resour. Res.* **2010**, *46*, W12550. [[CrossRef](#)]
50. Abarca, E.; Carrera, J.; Sánchez-Vila, X.; Dentz, M. Anisotropic dispersive Henry problem. *Adv. Water Resour.* **2007**, *30*, 913–926. [[CrossRef](#)]
51. Voss, C.; Provost, A. *SUTRA a Model for Saturated-Unsaturated, Variable-Density Ground-Water Flow with Solute or Energy Transport*; US Geological Survey: Reston, VA, USA, 2010.
52. Oswald, S.; Kinzelbach, W. Three-dimensional physical benchmark experiments to test variable-density flow models. *J. Hydrol.* **2004**, *290*, 22–42. [[CrossRef](#)]
53. Abarca, E.; Clement, T.P. A novel approach for characterizing the mixing zone of a saltwater wedge. *Geophys. Res. Lett.* **2009**, *36*, L06402. [[CrossRef](#)]
54. Walther, M.; Delfs, J.O.; Grundmann, J.; Kolditz, O.; Liedl, R. Saltwater intrusion modeling: Verification and application to an agricultural coastal arid region in Oman. *J. Comput. Appl. Math.* **2012**, *236*, 4798–4809. [[CrossRef](#)]
55. Mosegaard, K. Quest for consistency, symmetry, and simplicity—The legacy of Albert Tarantola. *Geophysics* **2011**, *76*, W51–W61. [[CrossRef](#)]
56. Darvini, G.; Salandin, P. Interazione tra acqua dolce e acqua salata in un acquifero costiero. In *Proceedings of the XXVIII Convegno di Idraulica e Costruzioni Idrauliche*, Potenza, Italy, 16–19 September 2002; Volume 2, pp. 129–138.